Chinese Journal of Catalysis 74 (2025) 108–119

available at www.sciencedirect.com

ScienceDirect

journal homepage: www.sciencedirect.com/journal/chinese-journal-of-catalysis

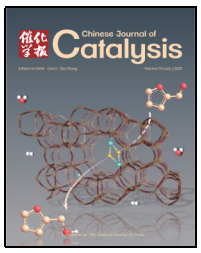

Article

Understanding the reaction-induced restructuring of CoO_x species in silicalite-1 to control selectivity in non-oxidative dehydrogenation of propane

Qiyang Zhang [a,*], Vita A. Kondratenko [a], Xiangnong Ding [a], Jana Weiss [a], Stephan Bartling [a], Elizaveta Fedorova [a], Dan Zhao [a,b,c], Dmitry E. Doronkin [b], Dongxu Wang [d], Christoph Kubis [a], Evgenii V. Kondratenko [a,*]

[a] *Leibniz-Institut für Katalyse e.V., D-18059 Rostock, Germany*
[b] *Institute for Chemical Technology and Polymer Chemistry, and Institute of Catalysis Research and Technology, Karlsruhe Institute of Technology, D-76131, Karlsruhe, Germany*
[c] *National Engineering Laboratory for Methanol to Olefins, Dalian National Laboratory for Clean Energy, iChEM (Collaborative Innovation Center of Chemistry for Energy Materials), Dalian Institute of Chemical Physics, Chinese Academy of Sciences, Dalian 116023, Liaoning, China*
[d] *Max Planck Institute of Microstructure Physics, 06120 Halle, Germany*

ARTICLE INFO

Article history:
Received 28 January 2025
Accepted 8 March 2025
Available online 20 July 2025

Keywords:
Propane
Dehydrogenation
Propene
Cobalt
Mechanism

ABSTRACT

Non-oxidative dehydrogenation of propane (PDH) is an important route for large-scale on purpose propene production. Although cobalt-based catalysts are promising alternatives to currently used platinum- or chromium oxide-based catalysts, their further developments are hindered by the uncertainties related to the kind of the active sites involved in the desired and side reactions. To contribute to closing such a gap, we systematically investigate the role of oxidized CoO_x and metallic Co^0 species in the PDH reaction over catalysts based in Silicalite-1 with supported CoO_x species differing in their redox properties. C_3H_8 pulse experiments with sub-millisecond and second resolution at pulse sizes of about 13 and 2200 nmol, respectively, combined with in-depth catalyst characterization and PDH tests at different propane conversions enabled us to understand how the reaction-induced reduction of CoO_x affects product selectivity. Propane readily reacts with CoO_x to yield propene, carbon oxides and water. The formed Co^0 species show high activity to coking and cracking reactions. However, if the size of such species is below 2 nm, these undesired reactions are significantly hindered due to the coverage of the active sites by carbon-containing species. The remaining uncovered surface Co^0 sites selectively dehydrogenate propane to propene. The best-performing catalyst showed higher activity than a commercial-like K-CrO_x/Al_2O_3 and operated durable in a series of 10 dehydrogenation/regeneration cycles under industrial relevant conditions. The space time yield of propene formation of 0.97 $kg \cdot h^{-1} \cdot kg_{cat}^{-1}$ was achieved at 550 °C, 52% equilibrium propane conversion and 95% propene selectivity.

1. Introduction

Propene is one of the most important basic petrochemicals widely used for the production of polypropylene, solvents,

* Corresponding author. E-mail: Qiyang.Zhang@catalysis.de (Q. Zhang), Evgenii.kondratenko@catalysis.de (E. V. Kondratenko).
https://doi.org/10.1016/S1872-2067(25)64724-3

acrylic acid, etc. [1,2]. The conventional routes for the manufacture of this building block include steam or fluid catalytic cracking of different oil fractions [3], metathesis of ethene with 2-butenes [4–6], methanol to olefin [7] and non-oxidative propane dehydrogenation (PDH) [8–10]. The PDH approach has been attracting increasing attention because of the shale gas revolution. This reaction is carried out on a large scale using highly expensive or environmentally unfriendly Pt- or Cr-containing catalysts [1]. Extensive efforts have been made to develop cheaper and more environmentally compatible alternatives. In this respect, oxide catalysts based on non-noble metals, including Zn [11–13], Zr [14,15], Mo [16], V [17,18], Ga [19,20], Co [21,22], are among the most promising candidates.

Co-based catalysts are of particular interest due to their excellent ability to selectively activate C–H bonds in various alkanes [23,24]. However, the kind of the active species (Co^0, Co^{2+} or Co_3O_4) responsible for the formation of propene in the PDH reaction is still controversially discussed in literature. Isolated $Co^{2+}O_x$ species on the surface of SiO_2 [25,26], Al_2O_3 [27] or zeolites [28,29] are widely accepted to be required for the desired reaction, while metallic Co^0 species catalyze cracking reactions of propane and coke formation [30,31]. However, other studies [30,32] suggest that the highly dispersed Co^0 species formed in situ from CoO_x dehydrogenate propane to propene selectively. A few efforts have been made to understand the role of metallic Co^0 in the PDH reaction. Recently, Li *et al*. [32] reported that small metallic Co^0 species formed from large Co^0 particles under reduction-reoxidation treatments show high dehydrogenation activity while their precursors tend to catalyze coking and cracking reactions. Yuan *et al*. [30] prepared ultrasmall CoO_x particles confined in the silanol nests of dealuminated beta zeolite and concluded that Co^0 formed in situ was responsible for the selective dehydrogenation of propane to propene. Yun *et al*. [33] reported that both Co^0 and tetrahedral $Co^{2+}O_x$ on the surface of Co/Al_2O_3 are active in the PDH reaction, with the latter being more selective. Since CoO_x can be reduced to Co^0 at high temperatures required for the PDH reaction, such contradictive statements regarding the role of Co^0 are detrimental to the rational development of Co-based catalysts and motivate further studies.

Against the above background, a series of Co-containing catalysts differing in CoO_x speciation were prepared using Silicalite-1 as a support. The purpose was to elucidate the role of acidic, redox, and structural properties of CoO_x species on their PDH performance. To be successful in this regard, the catalysts were characterized by complementary techniques including X-ray diffraction (XRD), temperature programmed desorption of ammonia (NH_3-TPD), temperature programmed reduction with hydrogen (H_2-TPR), transmission electron microscopy (TEM), ultraviolet-visible (UV-vis), Raman, X-ray photoelectron spectroscopy (XPS) and X-ray absorption spectroscopy (XAS). Further mechanistic insights into the role of different oxidation states of cobalt in product formation were derived by temporal analysis of products with sub-millisecond and second resolution. The results obtained provide a comprehensive basis for the development of industrially relevant Co-containing PDH catalysts as supported by the high performance of the best-performing catalyst developed in this study. It showed higher activity than an analogue of commercial of $K\text{-}CrO_x/Al_2O_3$ and was durable in a series of 10 dehydrogenation/regeneration cycles under industrially relevant conditions.

2. Experimental

2.1. Catalyst synthesis

Silicalite-1 (S-1) was prepared according to our previous work [13]. Briefly, TPAOH, TEOS and water were mixed with a mass ratio of TEOS:TPAOH:H_2O = 1:0.244:0.518, and stirred at room temperature for 6 h, followed by hydrothermal treatment at 100 °C for 48 h. After cooling down to room temperature, the formed solid material was separated by centrifugation, and then washed with deionized water and dried at 100 °C. Finally, the obtained solid material was calcined at 550 °C for 6 h to yield the S-1 support. Co/S-1 catalysts with different Co amounts were prepared by incipient impregnation method using an aqueous solution of $Co(NO_3)_2{\cdot}6H_2O$ followed by drying at 100 °C for 12 h and calcination in air at 550 °C for 4 h. The samples obtained were denoted as *x*Co/S-1, where "*x*" is the weight percentage of cobalt.

An analogue of the commercial $K\text{-}CrO_x/Al_2O_3$ catalyst was prepared according to the protocol described in the literature [34]. Briefly, two aqueous solutions with the required amounts of CrO_3 and KOH were separately prepared and then mixed. Hereafter, Al_2O_3 (Saint-Gobain NorPro) was impregnated with the resulting solution. The catalyst precursor was dried at 120 °C overnight and calcined at 760 °C for 4 h. The nominal concentrations of Cr_2O_3 and K_2O in the resulting catalyst are 19.7 and 0.93 wt% respectively.

2.2. Catalyst characterization

XRD patterns of as prepared catalysts were recorded using a Bruker D8 Advance diffractometer operating with Cu *Kα* radiation (0.15406 nm) at 40 kV and 100 mA.

UV-vis spectroscopy measurements were carried out using an Avantes spectrometer (AvaSpes-2048-USB2-RM) equipped with a high-temperature reflection UV-vis probe, an Ava-Light-DH-S-BAL deuterium-halogen light source and a CCD array detector. The probe consisting of six radiating optical fibers and one reading fiber was threaded through the furnace to face the wall of the quartz tubular reactor at the position where the catalyst (100 mg) was positioned. The UV-vis spectra were recorded at room temperature in the range from 200–1000 nm. Barium sulfate (99.998%, Aldrich) was used as a white standard. For operando UV-vis tests, 1Co/S-1 was heated in N_2 from room temperature to 550 °C followed by pulsing a mixture with 5 vol%C_3H_8 in Ar using a loop of 1 mL. The relative reflectance (R_{rel}) defined as the ratio of the reflectance of 1Co/S-1 under PDH conditions to that of the fully oxidized catalyst was used to calculate the relative Kubelka-Munk function $F(R_{rel})$ using Eq. (1).

$$F(R_{rel}) = \frac{(1-R_{rel})^2}{2\times R_{rel}} \quad (1)$$

High-resolution TEM (HRTEM) images were recorded on an FEI Talos 200X with a working voltage of 200 kV.

X-ray absorption spectra at the Co K absorption edge were recorded at the P65 beamline of PETRA III synchrotron radiation source (DESY, Hamburg) in transmission mode. Higher harmonics were rejected by a pair of Si plane mirrors installed in front of the monochromator. The energy of the X-ray photons was further selected by a Si(111) double-crystal monochromator and the beam size was set by means of slits to 0.3 (vertical) x 2.0 (horizontal) mm^2. The spectra were normalized and the extended X-ray absorption fine structure spectra (EXAFS) background was subtracted using the ATHENA program from the IFEFFIT software package [35]. The k^2-weighted EXAFS functions were Fourier transformed (FT) in the k range of 3.0–8 $Å^{-1}$ and multiplied by a Hanning window with sill size of 1 $Å^{-1}$. The FT EXAFS spectra were not corrected for the phase shift. The fitting was performed in the r-space on k^1, k^2-weighted data in the r-range of 1.0–3.5 Å. Co foil as a reference compound was used to establish the value of the reduction factor S_0^2. For this purpose, the correlation between S_0^2 and the σ^2 was determined under differently weighted functions $k^n\chi(k)$ (n = 0, 1, 2), which was obtained from modeling the first coordination sphere of Co foil. The crossing region of these curves was centered to obtain the value.

H_2-TPR were carried out in an in-house developed setup containing eight individually heated continuous-flow fixed-bed quartz reactors. This set-up was also used for NH_3-TPD and temperature-programmed surface reaction (C_3H_8-TPSR) measurements with C_3H_8.

For H_2-TPR tests, 100 mg of each sample was heated in flowing air to 500 °C for 1 h, cooled down to room temperature and purged with Ar for 15 min. Hereafter, the catalysts were heated in a flow of 5 vol% H_2 in Ar (10 mL·min^{-1}) up to 900 °C with a heating rate of 10 K·min^{-1}. An on-line mass spectrometer (Pfeiffer Vacuum OmniStar GSD 320) was used to record signals at m/z of 2 (H_2) and 40 (Ar), with the latter one being a reference standard.

Before NH_3-TPD tests, each sample (50 mg) was calcined in flowing air at 550 °C for 1 h, flushed with Ar (10 mL·min^{-1}) for 15 min, reduced with 40 vol% H_2/Ar (10 mL·min^{-1}) for 30 min, cooled down to 120 °C, and finally purged with Ar for 15 min. Hereafter, the treated materials were exposed to a flow of 1 vol% NH_3 in Ar (10 mL·min^{-1}) at 120 °C for 1 h, flushed with Ar for 5 h to remove weakly bound NH_3 at the same temperature, and then cooled down to 80 °C in the same flow. Then, they were heated in Ar flow up to 900 °C with a heating rate of 10 °C·min^{-1}. Desorbed ammonia was monitored using an on-line mass spectrometer (Pfeiffer Vacuum OmniStar GSD 320). The signals at m/z of 15 (NH) and 40 (Ar) were recorded.

Before starting C_3H_8-TPSR tests, all catalysts (50 mg for each sample) were calcined at 500 °C in flowing air for 1 h and then cooled down to 300 °C. Hereafter, the catalysts were flushed with Ar for 30 min and then exposed to a flow of C_3H_8/Ar = 10/90 (10 mL·min^{-1}). The temperature was initially kept at 300 °C for 15 min to obtain stable mass spectroscopic signals. Then, the catalysts were heated up to 600 °C with a heating rate of 10 °C·min^{-1}. The signals at m/z of 44 (C_3H_8), 42(C_3H_6), 18 (H_2O), 16 (CH_4), 2 (H_2), and 40 (Ar) were collected. The contribution of propane to propene and methane signals was separately determined using a calibration mixture with 10 vol% C_3H_8 in Ar and subtracted from the overall signals at m/z of 42 and 16.

Pseudo in situ XPS measurements were performed in a laboratory Near Ambient Pressure X-ray photoelectron spectroscopy system (NAP-XPS, SPECS Surface Nano Analysis GmbH, Germany). The setup is equipped with a differentially pumped Phoibos 150 electron energy analyzer and a monochromated Al K_α radiation source (E = 1486.6 eV) operated at 70 W and 15 kV. The system is connected to a High-Pressure Cell (HPC 20, SPECS Surface Nano Analysis GmbH, Germany), which offers sample heating by a halogen lamp (up to 800 °C) and is equipped with 4 mass flow controllers at the gas inlet and a manual back pressure regulator (Swagelok, USA) at the outlet. For the current experiments at ambient pressure, a total flow of 50 mL·min^{-1} was used for the catalyst treatment with 40 vol% H_2 in N_2 at 550 °C for 30 min. After a given time on stream, the treated sample was cooled down in N_2 before the cell was evacuated and then transferred under vacuum to the measurement chamber. The powder samples are pressed on a stainless-steel sample plate using a laboratory press with 5 mm diameter and a load of about 1 ton. Temperature was monitored by a thermocouple on the sample plate pressed to the sample surface. The electron binding energies were obtained with charge compensation using a flood electron source and referenced to the Si $2p_{3/2}$ peak of SiO_2 at 103.3 eV. For quantitative analysis, the peaks were deconvoluted with Gaussian-Lorentzian curves using the software Unifit 2023.

The size of Co^0 particles and Co^0 dispersion on the surface of reduced 1Co/S-1 and 5Co/S-1 were calculated based on the amount of H_2 desorbed and reduction degree of CoO_x as follows. Each catalyst (100 mg) was initially heated to 550 °C in a flow of O_2/He = 1:4 (20 mL·min^{-1}) for 30 min, flushed with He (20 mL·min^{-1}) for 15 min, reduced with 40 vol% H_2/He (20 mL·min^{-1}) for 30 min, and then cooled down to 50 °C. Hereafter, the reduced catalysts were flushed with He for 12 h to remove weakly bound H_2 at the same temperature. Then, they were heated in He up to 550 °C with a heating rate of 10 °C·min^{-1}. The degree of reduction of CoO_x in the reduced catalysts was determined by O_2 pulse titration tests (the overall pulse size was 1 mL) at 550 °C using a 5 vol% O_2/He mixture to re-oxidize the reduced metallic cobalt. Desorbed H_2 and consumed O_2 were monitored using an on-line mass spectrometer (Pfeiffer Vacuum OmniStar GSD 350). The signals at m/z of 2 (H_2), 32 (O_2) and 4 (He) were recorded.

Operando Raman experiments were used to monitor the restructuring of the catalysts during the pretreatment and PDH reaction using a Renishaw inVia Raman microscope equipped with a 633 nm air cooled He Ne laser. The tests were conducted in a Linkam reaction cell with a ceramic reactor containing approximately 50 mg of the catalyst, resulting in a total filling height of about 4 mm. The laser beam was focused on the sample with a ×20 objective, whereby a laser power of no more than 1.7 mW was set to avoid fluorescence, sample damaging and still achieve sufficient band intensity. For calcination, the

catalysts were heated in He to 550 °C (10 °C·min^{-1}) before being exposed to synthesis air (10 mL·min^{-1}) for 30 min. After flushing with He for 15 min, the oxidized catalysts were exposed to 40 vol%C_3H_8/N_2 mixture (10 mL·min^{-1}) for 60 min. All gases were dosed by calibrated mass flow controllers. Spectra were collected at a defined temperature or duration of exposure, respectively.

2.3. C_3H_8-pulse experiments at ambient pressure

C_3H_8-pulse experiments were performed over oxidized and reduced 1Co/S-1 and 3Co/S-1 samples according to the following protocol. To investigate the oxidized catalyst, 100 mg of each sample were initially heated to 550 °C in a flow of O_2/Ar = 1:4 (10 mL·min^{-1}) for 30 min and then flushed with Ar for 20 min. Finally, an C_3H_8/Ar = 5:95 mixture was pulsed (the pulse size was 1 mL) 20 times. To analyze the reduced catalysts, 100 mg of each sample were initially calcined at 550 °C in flowing O_2/Ar = 1:4 (10 mL·min^{-1}) mixture for 30 min and then flushed with Ar for 20 min. Hereafter, the oxidized catalysts were exposed to a flow of H_2/Ar = 1:4 (10 mL·min^{-1}) for 30 min and flushed with Ar for 20 min. Finally, an C_3H_8/Ar = 5:95 mixture was pulsed (the pulse size was 1 mL) 20 times. The signals at m/z of 40 (Ar), 29 (C_3H_8), 41 (C_3H_6), 2 (H_2), 16 (CH_4) and 44 (CO_2) were recorded by an on-line mass spectrometer (Pfeiffer Vacuum OmniStar GSD 350).

2.4. Temporal analysis of products

Transient experiments with sub-millisecond resolution were performed in the temporal analysis of products (TAP-2) reactor system described in Refs. [36–38]. In these experiments, each catalyst (1Co/S-1 or 5Co/S-1, 30 mg, 315–715 μm fraction) was sandwiched between two layers of quartz particles (250–355 μm) within the isothermal zone of a quartz tube reactor. Prior to the experiments, the catalysts were treated either oxidatively or reductively. A fresh sample was used for each type of treatment. For the oxidative treatment, the catalysts were heated from room temperature to 550 °C in an O_2-containing flow (3 mL·min^{-1} of O_2 and 3 mL·min^{-1} of N_2) for 30 min. During the reductive treatment, the catalysts were first oxidized as described above. The reactor was then evacuated and finally exposed to a flow of H_2 (2 mL·min^{-1}) and N_2 (3 mL·min^{-1}) at the same temperature for 1 h. After evacuation to ca. 10^{-5} Pa, a C_3H_8:Ar = 1:1 mixture was pulsed at 550°C. The mixture was prepared using C_3H_8 (Linde, 3.5) and Ar (Air Liquide, 5.0) without additional purification.

The experiments were carried out with an overall pulse size of 1.2–2×10^{16} molecules. The feed components and the reaction products at the reactor outlet were identified using an on-line quadrupole mass spectrometer (HAL RC 301 Hiden Analytical). The following m/z values were monitored: 44 (CO_2, C_3H_8), 42 (C_3H_8, C_3H_6), 41 (C_3H_8, C_3H_6), 29 (C_3H_8), 28 (C_3H_8, C_2H_8, CO_2, CO), 26 (C_3H_8, C_3H_6, C_2H_8, C_2H_6), 18 (H_2O), 16 (CH_4), 2 (H_2) and 40 (Ar). The pulses for each m/z were repeated 10 times and averaged to improve the signal-to-noise ratio. The contribution of different compounds to a certain m/z value was estimated from standard fragmentation patterns, determined in separate experiments.

2.5. Propane dehydrogenation tests

All catalytic tests were carried out at 550 °C and 1 bar in an in-house developed setup consisting of 15 continuous-flow fixed-bed quartz reactors. Typically, the catalysts (25 mg, fraction of 315–710 μm) were heated to 550 °C in N_2 flow with a heating rate of 10 °C·min^{-1} and then treated in air for 1 h. Hereafter, they were flushed with N_2 for 15 min and exposed to a flow (40 mL·min^{-1}) of 40 vol% C_3H_8/N_2. To determine an apparent activation energy of propene formation in the temperature range of 500–545 °C, catalytic tests were carried out at propane conversion below 10%. To this end, the catalyst amount and the total feed flow were varied from 25 to 50 mg and from 10 to 40 mL·min^{-1}, respectively. The rate of propene formation was determined at a degree of propane conversion below 10% after the first 240 s on propane stream (Eq. (2)).

$$r(C_3H_6) = \frac{F_{feed} \cdot x_{C3H6}}{V_m \cdot m_{cat}} \quad (2)$$

where is F_{feed} the volumetric feed flow rate (mL·min^{-1}). x_{C3H6} is the mole fraction of C_3H_6. V_m and m_{cat} stand for the molar volume (22.4 mL·mmol^{-1}) and catalyst mass, respectively.

Durability of 1Co/S-1 was investigated in a series of 10 PDH/regeneration cycles performed at 550 °C using a 40 vol% C_3H_8/N_2 mixture (10 mL·min^{-1}). The catalyst amount was set to 100 mg. Prior to the first PDH cycle, the catalyst was heated to 550 °C in N_2 flow and then calcined in air for 1h. Each PDH cycle lasted for 120 min, while catalyst regeneration was performed at the same temperature in air flow and lasted for 30 min. The PDH and the regeneration cycles were separated by a purging step in N_2 flow for 15 min.

Eqs. (3)–(6) were used for calculating propane conversion ($X(C_3H_8)$), selectivity to gas-phase products (S_i) and space-time yield of propene formation ($STY(C_3H_6)$), as well as an apparent deactivation rate constant (k_d), respectively.

$$X(C_3H_8) = \frac{\dot{n}^{in}_{C_3H_8} - \dot{n}^{out}_{C_3H_8}}{\dot{n}^{in}_{C_3H_8}} \quad (3)$$

$$S_i = \frac{v_{C_3H_8}}{v_i} \times \frac{\dot{n}^{out}_i}{\dot{n}^{in}_{C_3H_8} - \dot{n}^{out}_{C_3H_8}} \quad (4)$$

$$STY_{(C_3H_6)} = \frac{F_{feed} \times x_{C3H6} \times M_{C3H6}}{1000 \times V_m \times m_{cat}} \quad (5)$$

$$k_d = \frac{\ln\frac{1-X_{end}}{X_{end}} - \ln\frac{1-X_{start}}{X_{start}}}{t} \quad (6)$$

$\dot{n}$ ($\dot{n}_i$ or $\dot{n}_{C3H8}$) with superscripts in or out stands for the mole flows of gas-phase reaction products or propane at the reactor inlet or outlet. Here, v_i is the stoichiometric coefficient for product i. MC_3H_6 stands for the molar weight of propene (42.08 g·mol^{-1}). N_2 was used as internal standard to consider reaction-induced changes in the number of moles. X_{start} and X_{end} stand for propane conversion after 4 min and 4 h on stream, respectively.

An on-line gas chromatograph (Agilent 6890) equipped with

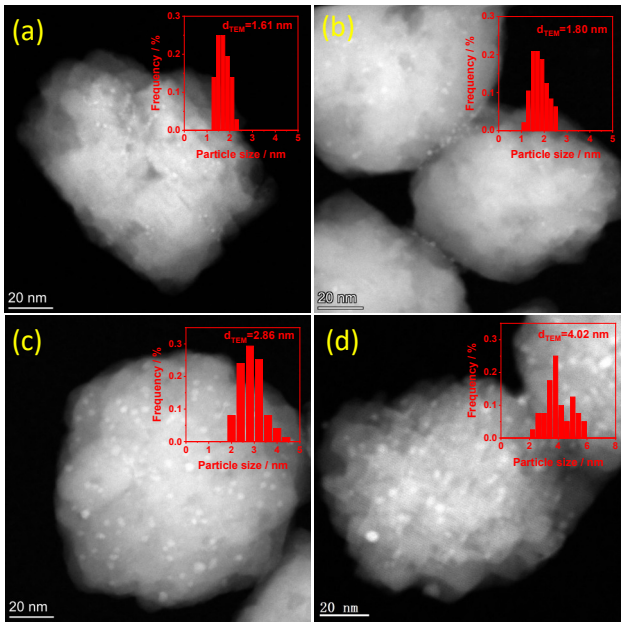

Fig. 1. HAADF-STEM images of as-prepared 0.6Co/S-1 (a), 1Co/S-1 (b), 3Co/S-1 (c), and 5Co/S-1 (d).

PLOT/Q (for CO_2), AL/S (for hydrocarbons), and Molsieve 5 (for H_2, O_2, N_2 and CO) columns as well as flame ionization and thermal conductivity detectors was used for quantifying the concentration of the feed components and the reaction products.

3. Results and discussion

3.1. Catalysts and their general characterization

High-angle annular dark-field scanning transmission electron microscopy (HAADF-STEM) was applied to analyze the effect of Co loading (0.6 wt%–5 wt%) on the size of supported CoO_x species (Fig. 1). As expected, the average size increased from 1.6 to 4 nm with an increase in the loading from 0.6 to 5 wt% (see inserts in Fig. 1). No crystalline Co-containing phase(s) could be identified in the 0.6Co/S-1 and 1Co/S-1 catalysts, while a diffraction peak at 2θ =36.9° characteristic of Co_3O_4 (see Ref. [33]) appeared in the XRD patterns of higher loaded catalysts (Fig. S1(b)). The difference between these two catalyst groups should be related to the size of supported CoO_x. X-ray amorphous Co_3O_4 could be identified in the 0.6Co/S-1 and 1Co/S-1 catalysts as can be concluded from the UV-vis spectra displaying two bands at around 445 and 740 nm typical for this cobalt oxide (Fig. 2(a)) [9]. Additional bands at around 497, 542 and 667 nm present in the spectra of all catalysts can be attributed to divalent of Co [28].

For the 5Co/S-1 and 3Co/S-1 samples, their XANES spectra look similar to that of Co_3O_4 (Fig. 2(b)), indicating the presence of this cobalt oxide as also proven by our XRD analysis (Fig. S1(b)). In the case of the samples with lower Co loading, the intensity of the main edge peak at 7724.6 eV (marked with * in Fig. 2(b)) increases, which could be explained by the presence of Co_3O_4 nanoparticles with a smaller size [39]. According to the fit of the EXAFS spectra (Fig. 2(c), Fig. S2), a Co–O–Co bond assigned to Co_3O_4 was identified [27]. The higher the Co–O–Co coordination numbers (CNs), the bigger the Co_3O_4 size [40]. The fitted CNs of 0.6Co/S-1 and 1Co/S-1 are 4.7 and 5.4, respectively. These values are lower than 9.2 and 8.9 obtained for 3Co/S-1 and 5Co/S-1, respectively.

3.2. Redox behavior of supported CoO_x species

The reducibility of the fresh *x*Co/S-1 catalysts was investigated by H_2-TPR. The reduction process starts at a relatively low temperature, depending on the Co loading (Fig. 3(a)). Only one H_2 consumption peak between 354–325 °C was identified in the H_2-TPR profiles of 0.6Co/S-1 and 1Co/S-1 and was attributed to the reduction of Co_3O_4 to metallic Co, which looks like a "single-step" process because the unstable CoO as intermediate is typically unseen upon reduction of small sized Co_3O_4 domains [41]. Noticeably, two obvious H_2 consumption peaks are present in the H_2-TPR profiles of 3Co/S-1 (335 and 384 °C) and 5Co/S-1 (353 and 453 °C), possessing large crystalline Co_3O_4 species. In agreement with Ref. [42], the following reduction processes Co_3O_4→CoO→Co should be valid for these two catalysts.

The presence of Co^0 was confirmed directly by quasi in situ XPS measurements performed after reduction of 1Co/S-1 in 40 vol% H_2 in N_2 at 550 °C for 30 min (Fig. 3(b)). Whereas only Co^{2+} with its characteristic satellite features [43] was identified in the calcined catalyst, a pronounced Co^0 peak at 777.6 eV [43] was observed after reduction treatment at 550 °C. As the reduction ability of propane is even stronger than that of H_2, Co^0 species should also be formed *in situ* during the PDH reaction.

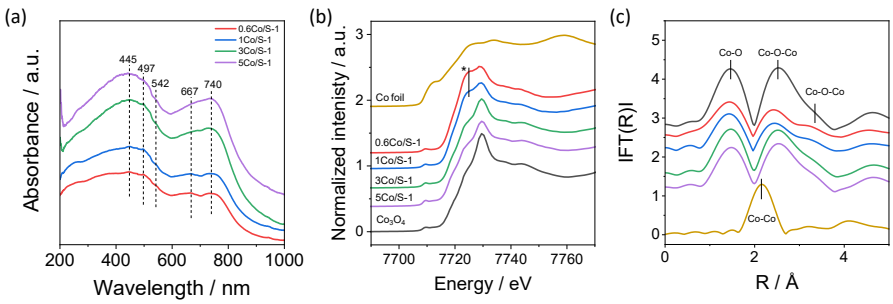

Fig. 2. UV-vis spectra (a) and Co K-edge XANES (b) of the fresh catalysts and reference samples (Co_3O_4 and Co foil). The corresponding k^2-weighted Fourier transform spectra are shown in (c).

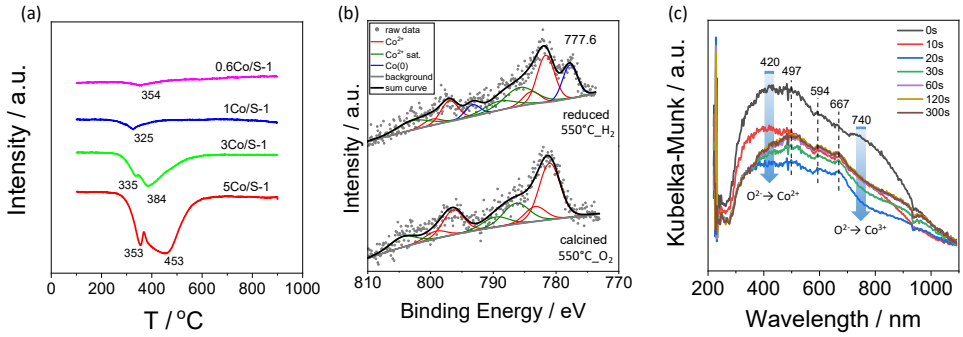

Fig. 3. (a) H_2-TPR profiles of *x*Co/S-1. (b) Quasi *in situ* XPS spectra of 1Co/S-1 after treatment at 550 °C with 20 vol% O_2/Ar or 40 vol% H_2/Ar. (c) In situ UV-vis spectra of 1Co/S-1 after treatment at 550 °C with 40 vol% H_2/Ar.

In situ UV-vis spectroscopy was applied to characterize the reduction of CoO_x species in 1Co/S-1 in a 40 vol% H_2/Ar flow at 550 °C (Fig. 3(c)). This reducing agent was used instead of C_3H_8 to avoid coke formation. The broad bands at 420 and 740 nm in the oxidized catalyst were assigned to the charge transfer transitions between O^{2-} and Co^{2+}, as well as between O^{2-} and Co^{3+}, respectively. An obvious decrease in the intensity of the bands could be observed during the first 20 s on H_2 stream. Based on the XPS data discussed above, the H_2-induced changes in the UV-vis spectrum can be interpreted as partial reduction of CoO_x to Co^0. The bands at 566, 594 and 667 nm can be ascribed to the $\nu_3(4A_2 \rightarrow {}^4T_1(P))$ transition characteristic of tetrahedral Co^{2+} species in the framework of zeolite [29]. They didn't disappear during the H_2 treatment, indicating that the tetrahedral Co^{2+} species were stable under treatment conditions.

3.3. Catalyst activity

The initial rate of propene formation over *x*Co/S-1 at 550°C is shown in Fig. 4(a). The conversion of propane in these tests was lower than 10% to ensure a differential reactor operation. The rate increased with increasing Co loading up to 1 wt% and reached its maximal value of 1.2 $mmol \cdot g^{-1} \cdot min^{-1}$. Noticeably, this activity level is higher as compared to a commercial analogue of K-CrO_x/Al_2O_3. When the cobalt loading was above 1 wt% the activity decreased obviously. The decrease might be due to the presence of crystalline Co_3O_4 in higher loaded catalysts as proven by HAADF-STEM and XRD (Fig. 1 and Fig. S1) [32].

Further insights into the effect of Co loading on PDH were derived from C_3H_8-TPSR in the temperature range of 300–600 °C (Fig. S3). The lowest initial propene formation temperature of 424 °C was determined for 1Co/S-1 (Fig. 4(b)), which is consistent with the highest activity of this catalyst under steady-state conditions (Fig. 4(a)). No obvious propene formation over 5Co/S-1 could be observed below 575 °C. For all

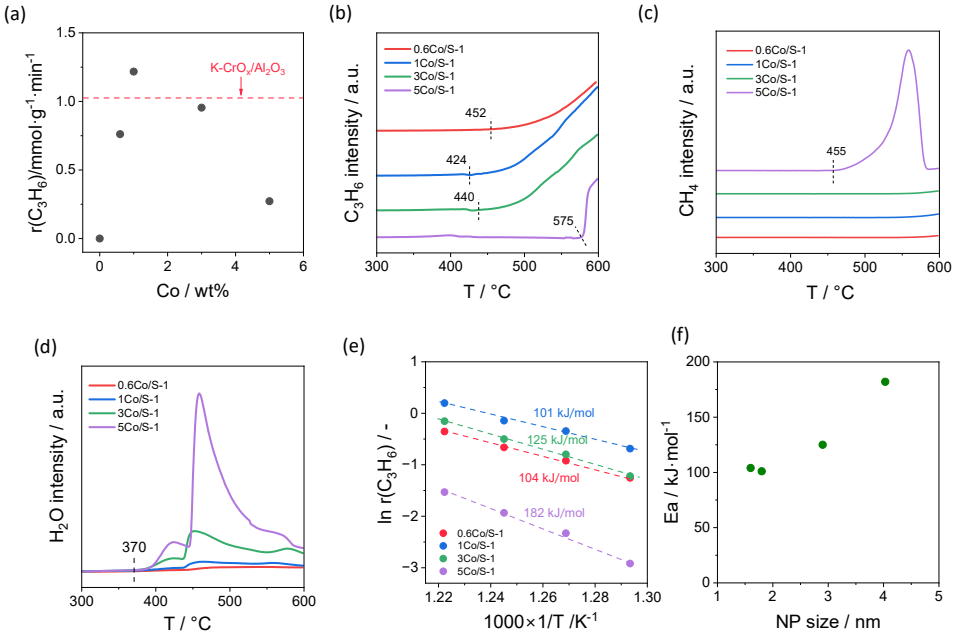

Fig. 4. (a) The rate of propene formation over *x*Co/S-1. Temperature-resolved *m*/*z* values of 42 (C_3H_6) (b), 16 (CH_4) (c) and 18 (H_2O) (d) collected during temperature-programmed surface reaction of C_3H_8 with *x*Co/S-1 between 300 and 600 °C. (e) Arrhenius plots of the propene formation rate over *x*Co/S-1 as well as the respective apparent activation energy (E_a). (f) E_a versus the size of CoO_x NP determined by HAADF-STEM (Fig. 1).

catalysts, H_2O was formed above 370 °C which is lower than the temperature of C_3H_6 formation (Fig. 4(b) and (d)). The formation of H_2O is a clear indicator for the removal of lattice oxygen from Co_3O_4 by propane, i.e. this oxide is reduced. H_2 was also formed in the C_3H_8-TPSR tests. This process started at higher temperatures than the formation of H_2O (Fig. S3, Fig. 4(d)). In addition to the above-mentioned products, methane was also formed to varying degrees depending on Co loading. The highest amounts were formed over 5Co/S-1 (Fig. 4(c)). Combined with the H_2-TPR results, Co^0 should be formed in situ during C_3H_8-TPSR. Based on the latter results and catalyst characterization by XAS (Fig. 2), HAADF-STEM (Fig. 1) and XRD (Fig. S1), small Co^0 particles should be active for the desired reaction, while Co^0 larger than 4 nm are active for cracking reactions.

Co loading in the catalysts is also relevant to the apparent activation energy (E_a) of propene formation determined from the rate of propene formation in the temperature range from 500 to 545 °C (Fig. 4(e)). Similar E_a values, i.e., 104 and 101 kJ·mol^{-1}, were found for 0.6Co/S-1 and 1Co/S-1, respectively. When the loading of Co was increased to 3 wt% and 5 wt%, E_a also increased to 125 and 182 kJ·mol^{-1}, respectively. These results indicate that the catalysts with smaller Co^0 particles have lower E_a and higher intrinsic activity for propene formation (Fig. 4(f)).

3.4. Reaction pathways of products formation

Having identified the effects of Co loading on catalyst activity, we also analyzed the selectivity-conversion relationships for C_3H_6, C_1–C_2 hydrocarbons (cracking products) and coke to check if and how the loading affects primary and secondly reaction pathways in the course of PDH. The conversion was varied by changing both catalyst amount and total feed flow, while the reaction temperature and the feed composition were constant. For all catalysts, the selectivity to propene decreases with increasing propane conversion (Fig. 5(a)). An opposite trend was found for the selectivity to cracking products and coke (Fig. 5(b) and 5(c)). Such results indicate that propene is formed directly from propane and is further converted into coke and cracking products. When the selectivity to C_1–C_2 hydrocarbons was extrapolated to zero propane conversion, a zero value was obtained (Fig. 5(b), Fig. S4). Thus, these products should not be additionally formed directly from C_3H_8 but originate from C_3H_6 exclusively as can be concluded from the decrease in the selectivity to the latter product with increasing propane conversion. A near-zero selectivity to coke at zero propane conversion was also obtained for the 0.6Co/S-1 and 1Co/S-1 catalysts (Fig. 5(c), Fig. S4). Similar to C_1–C_2 hydrocarbons, coke should be formed from propene but not from propane. These conclusions are indirectly supported by close to 100% propene selectivity extrapolated to zero propane conversion. Such selectivity value of 3Co/S-1 is lower suggesting the presence of direct pathways of propane conversion to C_1-C_2 hydrocarbons and coke. Nevertheless, the main routes leading to these products involve propene. These reactions are favored by large CoO_x particles. Based on the above discussion, two possible reaction networks of propane dehydrogenation were proposed for 0.6Co/S-1and 1Co/S-1 (Fig. 5(d)) as well as 3Co/S-1 (Fig. 5(e)).

Since catalyst acidity is usually considered to be the most important catalyst property affecting coke formation and selectivity to cracked products, we also tried to see if such a correlation held true for our catalysts. No obvious correlation was obtained between the selectivity to these products and the acidity of the catalysts determined from NH_3-TPD tests (Figs. S5–S6, Table S2). Therefore, the selectivity difference should be mainly related to the size of metallic Co^0.

3.5. The kind of Co-containing species involved in the formation of propene and side products

To investigate the ability of oxidized supported CoO_x species to oxidatively dehydrogenate propane, two series of pulse experiments with C_3H_8 were performed using the 1Co/S-1 and 5Co/S-1 catalysts under different pressure conditions. The very early catalyst performance without significant changes in the oxidation state of CoO_x during a pulse was analyzed using a Temporal Analysis of Products (TAP) reactor [36–38], which operates in high vacuum with sub-millisecond resolution. In these experiments the amount of pulsed propane in one pulse was about 13 nmol. In the tests performed at ambient pressure with a second resolution using a conventional pulse reactor, the propane pulse size was about 2200 nmol. We start our discussion with the results of TAP tests.

When a C_3H_8:Ar = 1:1 mixture was pulsed over the oxidized 1Co/S-1 or 5Co/S-1 catalysts at 550°C H_2O, CO_2 and CO were formed (Figs. 6(a) and (d)). Additionally, the formation of C_3H_6 and H_2 was observed over 1Co/S-1. For better distinguishing between the responses corresponding to the substances with different molecular masses the experimental time was trans-

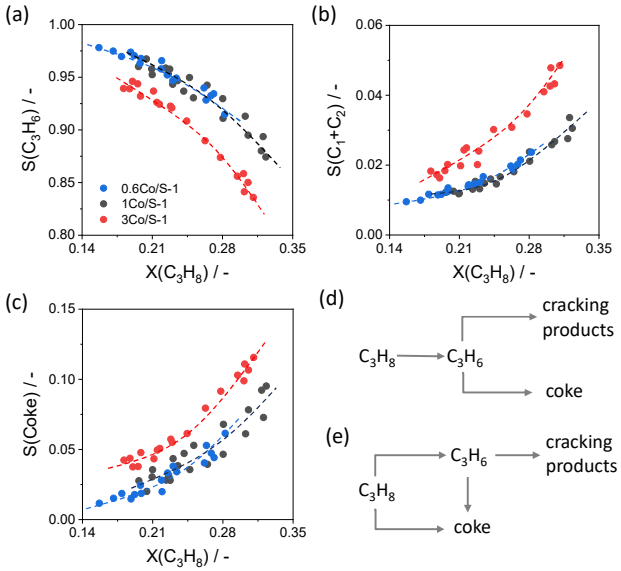

Fig. 5. The selectivity-conversion relationships for propene (a), C_1-C_2 hydrocarbons (b) and coke (c) formed over 0.6Co/S-1, 1Co/S-1 and 3Co/S-1. Proposed reaction pathways for propane dehydrogenation over 0.6Co/S-1 and 1Co/S-1 (d) as well as 3Co/S-1 (e). Reaction conditions: T = 550 °C, C_3H_8:N_2 = 2:3, WHSV(C_3H_8) = 2.4–14.1 h^{-1}.

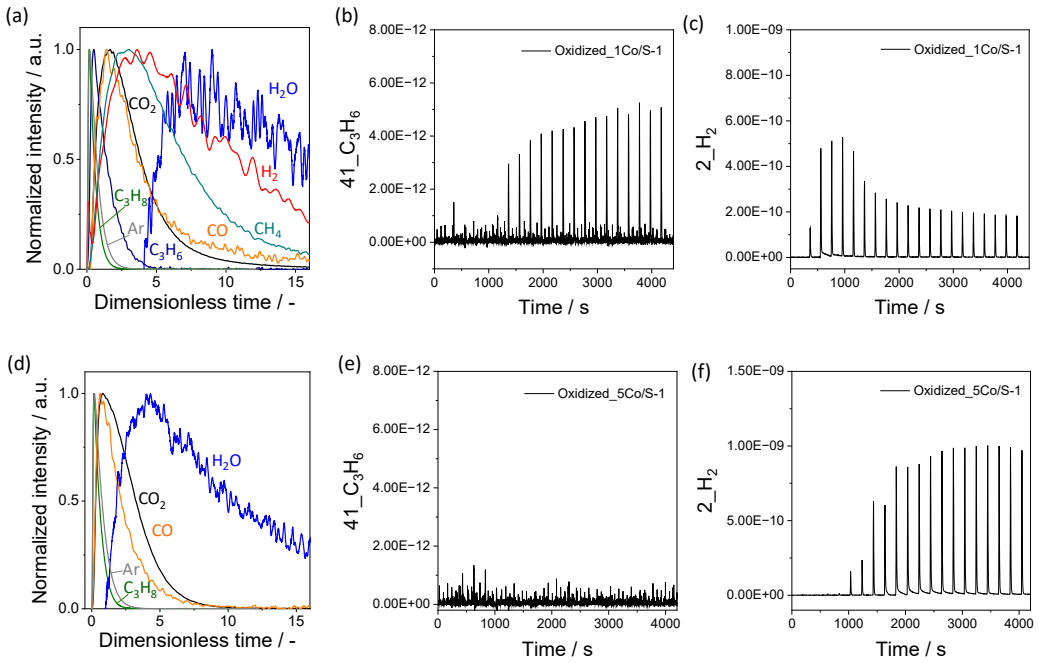

Fig. 6. The normalized transient responses recorded upon pulsing a C_3H_8:Ar = 1:1 mixture at 550 °C over oxidized 1Co/S-1 (a) and 5Co/S-1 (d). C_3H_6 (b,e) and H_2 (c,f) response recorded at 550 °C after pulsing (1mL) of a C_3H_8/Ar = 1:19 mixture over oxidized 1Co/S-1 (b,c) and 5Co/S-1 (e,f). Before the C_3H_8 pulses, the catalysts were exposed to a flow of O_2/Ar = 1:4 (10 mL·min^{-1}) at 550 °C for 30 min and then flushed with Ar for 20 min.

formed into a dimensionless time as suggested in Ref. [44]. The formation of oxygen-containing products indicates that the lattice oxygen of the CoO_x species has been consumed in the reaction with propane, resulting in the reduction of CoO_x species. The absence of C_3H_6 and H_2 in the product spectrum in the test with 5Co/S-1 indicates that large CoO_x species provide significantly higher amount of lattice oxygen as compared to the amount of pulsed propane, which is favorable for deep oxidation reactions (Fig. 6(d)).

In agreement with the TAP results discussed above, C_3H_6, H_2, CO_2 and CH_4 were formed over oxidized 1Co/S-1 in the first C_3H_8 pulse (a C_3H_8:Ar = 1:19 mixture) at 550 °C and ambient pressure (Figs. 6(b) and (c), Fig. S7). However, H_2 was the only gas-phase product detected in the second to fourth C_3H_8 pulses. The difference between these tests and the TAP tests should be related to the amount of propane pulsed. The amount in the first propane pulse was about 440 times higher as compared to the total amount of propane pulsed in the whole TAP tests. The absence of any carbon-containing gas-phase products in the second to fourth propane pulses suggest that propane was decomposed to coke and hydrogen. Propene started to be formed again from the fifth pulse. Its concentration increased with increasing number of propane pulses. This induction period in the formation of propene suggests that selective Co-containing species are formed in situ and carbon-containing species play an important role. As recently reported in Ref. [45], a carbon-containing layer on oxidized CoO_x species can modify their performance.

For oxidized 5Co/S-1, only CH_4 and CO_2 were formed in the first four C_3H_8 pulses (Fig. S8). H_2 appeared in the fifth pulse and its amount increased with increasing number of propane pulses (Fig. 6(f)). CO_2 disappeared after the eleventh C_3H_8 pulse, indicating that supported CoO_x species provided all available oxygen species (Fig. S8). In contrast to 1Co/S-1, propene was not observed during the whole (20 propane pulses) pulse experiment (Fig. 6(e)). H_2 and CH_4 were the only gas-phase products. Thus, large CoO_x species reduced in situ are active in cracking and complete dehydrogenation reactions rather than in the selective dehydrogenation to propene.

To validate the above conclusions about the role of metallic Co^0 species and carbon deposits, we performed a similar series of propane pulse tests using 1Co/S-1 and 5Co/S-1 reduced in H_2 at 550 °C for 30 min. According to the XPS results, the reductively treated catalysts should contain metallic Co^0. The particle size of Co^0 species on the surface of reduced 1Co/S-1 and 5Co/S-1 was determined to be 2.0 and 4.5 nm, respectively (Figs. S9–S10; Table S3). Regardless of the size of propane pulse, no propene formation could be observed in the tests with reduced 5Co/S-1 (Figs. 7(d)–(f), Fig. S12(b)) although propane conversion at ambient pressure tests was close to 100% (Fig. S12(a)). The only gas-phase product observed over 5Co/S-1 was H_2 (Fig. 7(d)). C_2H_4, CH_4 and H_2 were formed over reduced 1Co/S-1 in the TAP tests (Fig. 7(a)). Importantly, the total amount of propane pulsed in this test was too low to change the state of metallic Co^0 species. Thus, the latter species or partially reduced CoO_x cannot be the selective sites responsible for the formation of propene from propane. This statement was supported by the results of pulse tests at ambient pressure performed with pulse sizes significantly higher than those of the TAP tests. In agreement with the above TAP results, no propene and methane were detected over reduced 1Co/S-1 in the first two propane pulses (Fig. 7(b), Fig. S11),

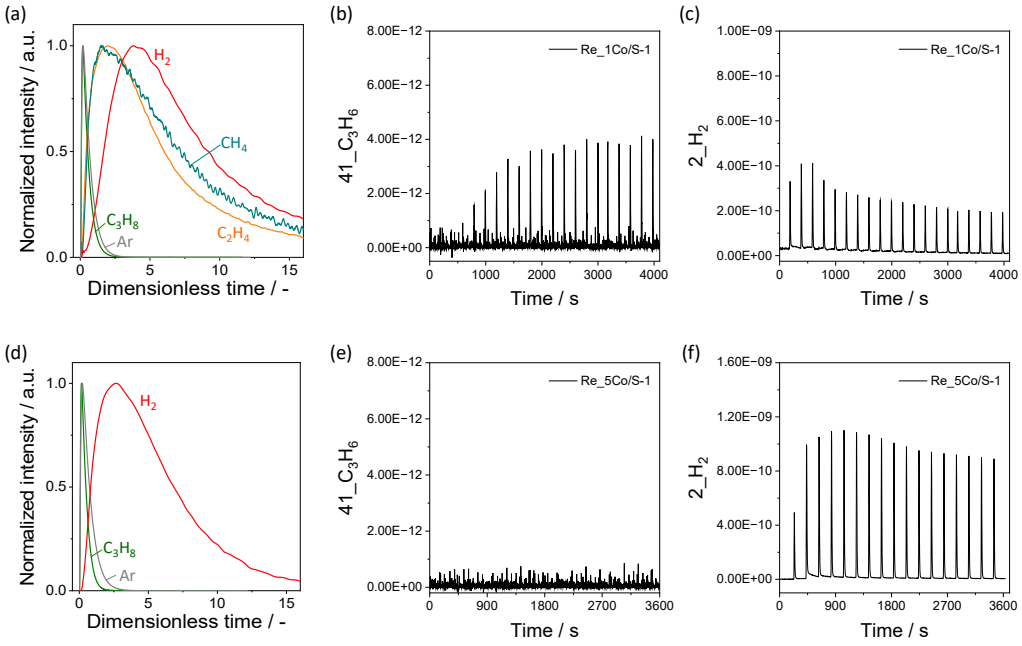

Fig. 7. The normalized transient responses recorded upon pulsing of a C_3H_8:Ar = 1:1 mixture at 550 °C over reduced 1Co/S-1 (a) and 5Co/S-1 (d). C_3H_6 (b,e) and H_2 (c,f) response recorded at 550 °C after pulsing (1mL) of an C_3H_8/Ar = 1:19 mixture over reduced 1Co/S-1 (b,c) and 5Co/S-1 (e,f). Before the C_3H_8 pulses, the catalysts were exposed to a flow of H_2/Ar=1:4 (10 mL/min) at 550°C for 30 min and then flushed with Ar for 20 min.

while H_2 was formed (Fig. 7(c)). Carbon-containing deposits must also be formed. Propene was observed in the third pulse and its concentration increased with increasing number of propane pulses (Fig. 7(b)). The concentration of hydrogen decreased indicating that the formation of coke also decreased (Fig. 7(c)).

To confirm the formation of coke over reduced 1Co/S-1 during large C_3H_8 pulses at ambient pressure, we used operando UV-vis spectroscopy. The obtained UV-vis spectra expressed as the relative Kubelka-Munk function (F(Rel)) are shown in Fig. 8(a). F(Rel) increases across the entire range of wavelengths, which is attributed to the presence of coke deposits. The strongest changes occurred during the first two C_3H_8 pulses and became less pronounced as the number of C_3H_8 pulses increased, due to the saturation of the sites responsible for carbon deposition. To provide an additional experimental support for the presence of carbon-containing species, the spent 1Co/S-1 catalyst after 20 C_3H_8 pulses was characterized by HRTEM. An amorphous carbon-layer on a metallic Co^0 particle was observed (Fig. S13).

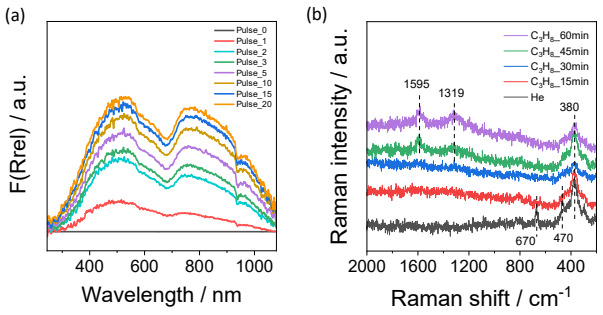

Fig. 8. (a) Operando UV-vis spectra of 1Co/S-1 during the C_3H_8 pulses (1mL pulse size) at 550 °C using a feed with 5 vol% C_3H_8 in Ar. (b) Operando Raman spectra of 1Co/S-1 collected during exposure to a feed with 40 vol% C_3H_8 in N_2 at 550 °C.

The operando Raman spectra (Fig. 8(b)) exhibits two weakly intense bands at 670 and 470 cm^{-1}, which can be unambiguously assigned to Co_3O_4 [46]. In addition, a relatively strong band at approximately 380 cm^{-1} is observed, which is likely derived from the silicalite-1 support [47]. The Co_3O_4 Raman peaks disappeared after the catalysts were exposed to a 40 vol%C_3H_8/N_2 mixture at 550 °C suggesting the reduction of this metal oxide. After 45 min on propane stream, the Raman spectrum of 1Co/S-1 was characterized by the appearance of weak G and D bands at around 1595 and 1319 cm^{-1} representative for the carbon species [48].

In summary, the lattice oxygen of oxidized CoO_x can oxidize propane not only to propene but also to carbon oxides. The larger the CoO_x species, the more important the latter reaction. Due to the limited amount of lattice oxygen species, these oxidation reactions proceed during a few first seconds on propane stream under PDH conditions and, thus, cannot be responsible the formation of propene in the PDH reaction. The propane-mediated reduction of CoO_x results in the formation of Co^0 species, which are, however, highly active for the conversion of propane to carbon-deposits, methane, and hydrogen but not to propene. To favor the latter reaction, small Co^0 species must be decorated by a carbon-containing layer, which simply covers the sites for the deep dehydrogenation and cracking reactions and/or changes the electronic state of Co^0 species requiring for the efficient dehydrogenation of propane to propene.

3.6. Industrial relevance and comparison with state-of-the-art

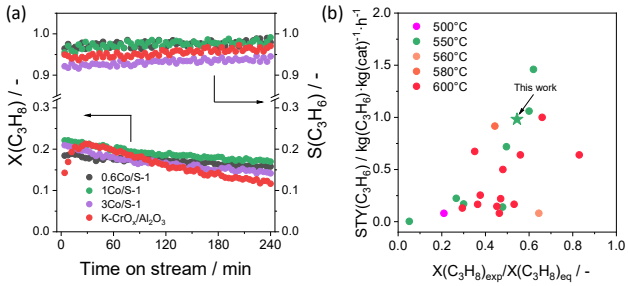

Fig. 9. (a) Time-on-stream profiles of propane conversion and propene selectivity over tested samples. (b) Space time yield of propene formation ($STY(C_3H_6)$) determined over 1Co/S-1 and previously reported Co-based catalysts (Table S4) versus $X(C_3H_8)_{exp}/X(C_3H_8)_{eq}$. Reaction conditions: T = 550 °C, catalyst amount = 100 mg, $WHSV(C_3H_8)$ = 4.7 h^{-1}, C_3H_8:N_2 = 2:3.

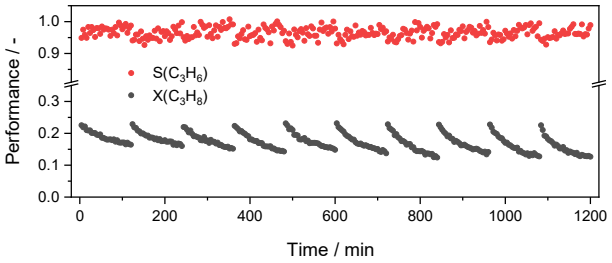

Fig. 10. Propane conversion and propene selectivity over 1Co/S-1 in 10 PDH/ regeneration cycles. Reaction conditions: T = 550 °C, catalyst amount = 100 mg, $WHSV(C_3H_8)$ = 4.7 h^{-1}, C_3H_8:N_2 = 2:3. Each cycle consisted of a PDH stage lasted for 120 min and a regeneration stage lasted for 30 min.

catalysts

The developed xCo/S-1 catalysts and a commercial analogue of K-CrO_x/Al_2O_3 were tested under industrially relevant conditions in parallel to ensure their direct comparison. They showed both higher propane conversion and propene selectivity (Fig. 9(a)). In addition, *x*Co/S-1 catalysts also deactivated slower during 240 min on propane stream. The deactivation rate constant of K-CrO_x/Al_2O_3 was determined to be 0.21 h^{-1}. The corresponding values of the *x*Co/S-1 are lower and decrease with decreasing Co loading, with the lowest value of 0.05 h^{-1} being determined for the 0.6Co/S-1 catalyst (Fig. S14).

We also benchmarked the most active 1Co/S-1 catalyst against Co-based catalysts reported in previous studies in terms of space-time-yield of propene formation ($STY(C_3H_6)$). To ensure an unbiased comparison of the catalysts tested under different reaction conditions, we plotted the $STY(C_3H_6)$ values versus the ratio of experimentally measured propane conversion to the corresponding equilibrium conversion ($X(C_3H_8)_{exp}/X(C_3H_8)_{eq}$). In general, the closer this ratio is to 1, the lower the $STY(C_3H_6)$ values will be obtained due to integral reactor operation and approaching to the equilibrium. Thus, industrially relevant catalysts should show high productivity at $X(C_3H_8)_{exp}/X(C_3H_8)_{eq}$ values as close to 1 as possible. The initial $STY(C_3H_6)$ value of the 1Co/S-1 catalyst of 0.97 $kg{\cdot}kg_{cat}^{-1}{\cdot}h^{-1}$ was achieved at 52% equilibrium propane conversion at 550 °C (Fig. 9(b)). Only two previously reported Co-containing catalysts showed comparable or slightly higher performance at 550 °C, while other catalysts showed lower activity despite having been tested at higher temperatures.

Finally, the practical relevance of the 1Co/S-1 catalyst was demonstrated in a series of 10 dehydrogenation/regeneration cycles under industrially relevant conditions (Fig. 10). The reaction was performed at 550 °C and lasted for 120 min using a feed with 40vol% C_3H_8. Hereafter, the catalyst was simply treated in air at the same temperature for 30 min. In all dehydrogenation cycles, although the conversion gradually decreased due to coke formation the initial conversion (about 23%) and propene selectivity (about 95%) values could be fully recovered after the oxidative catalyst treatment. The high productivity and durability of the catalysts developed in the present study further underline the potential of Co-based catalysts for PDH.

4. Conclusions

In this work, we have elucidated mechanistic aspects of the reaction-induced restructuring of CoO_x species supported on S-1 and its consequences for catalyst activity and, in particular, product selectivity in the PDH reaction. We have combined in situ XPS, in situ UV-vis and *in situ* Raman spectroscopy studies with continuous flow and pulse PDH tests. It is highly important to perform kinetic and characterization analysis at times ranging from milliseconds to minutes to derive insights into the kind of the active sites responsible for the formation of propene and side products. Based on the results obtained, we defined three stages in the course of the PDH reaction.

(1) Regardless of the size (1.6–4 nm) of CoO_x species containing Co^{2+} and Co^{3+}, the PDH reaction starts with the oxidation of propane to propene and carbon oxides, with the selectivity to the latter increasing with the size. Because of these reactions, Co^{2+} and Co^{3+} are reduced by to metallic Co^0.

(2) Freshly formed Co^0 species decompose propane to surface carbon-containing species and hydrogen as well as convert this alkane to C_1–C_2 hydrocarbons without the formation of propene. The sites responsible for these reactions are covered by carbon deposits resulting in hindering the undesired propane conversion.

(3) Co^0 species decorated by carbon deposits are required for the efficient dehydrogenation of propane to propene. The strength of the positive effect of such decoration increases with a decrease in the size of Co^0 species.

The obtained knowledge provides the basis for the rational development of efficient Co-containing catalysts by varying size and redox properties of supported CoO_x species.

Acknowledgments

Financial support by the State of Mecklenburg-Vorpommern is gratefully acknowledged. We acknowledge DESY (Hamburg, Germany), a member of the Helmholtz Association HGF, for the prevision of experimental facilities. Parts of this research were carried out at PETRA III, and we would like to thank Dr. Edmund Welter for assistance in using beamline P65. Beamtime

was granted for the proposal I-20230812.

Electronic supporting information

Supporting information is available in the online version of this article.

References

[1] S. Chen, X. Chang, G. Sun, T. Zhang, Y. Xu, Y. Wang, C. Pei, J. Gong, *Chem. Soc. Rev.*, **2021**, 50, 3315–3354.

[2] T. Otroshchenko, G. Jiang, V. A. Kondratenko, U. Rodemerck, E. V. Kondratenko, *Chem. Soc. Rev.*, **2021**, 50, 473–527.

[3] S. M. Sadrameli, *Fuel,* **2016,** 173, 285–297.

[4] Q. Zhang, T. Otroshchenko, E. V. Kondratenko, *Catal. Sci. Technol.,* **2022,** 12, 5210–5216.

[5] Q. Zhang, J. Rabeah, T. H. Vuong, T. Otroshchenko, E. V. Kondratenko, *Catal. Sci. Technol.,* **2023**, 13, 767–773.

[6] Q. Zhang, T. Xiao, C. Liu, T. Otroshchenko, E. V. Kondratenko, *Angew. Chem. Int. Ed.,* **2023**, 62, e202308872.

[7] M. Yang, D. Fan, Y. Wei, P. Tian, Z. Liu, *Adv. Mater.*, **2019**, 31, 1902181.

[8] Y. Li, Q. Zhang, S. Fu, V. A. Kondratenko, T. Otroshchenko, S. Bartling, Y. Zhang, A. Zanina, Y. Wang, G. Cui, M. Zhou, Z. Zhao, C. Xu, G. Jiang, E. V. Kondratenko, *Chem. Eng. J.*, **2023**, 460, 141778.

[9] Q. Zhang, Y. Li, T. Otroshchenko, V. A. Kondratenko, K. Wu, E. A. Fedorova, D. E. Doronkin, S. Bartling, H. Lund, G. Jiang, E. V. Kondratenko, *J. Catal.*, **2024**, 432, 115440.

[10] D. Zhao, X. Tian, D. E. Doronkin, S. Han, V. A. Kondratenko, J.-D. Grunwaldt, A. Perechodjuk, T. H. Vuong, J. Rabeah, R. Eckelt, U. Rodemerck, D. Linke, G. Jiang, H. Jiao, E. V. Kondratenko, *Nature*, **2021**, 599, 234–238.

[11] C. Chen, Z.-P. Hu, J.-T. Ren, S. Zhang, Z. Wang, Z.-Y. Yuan, *Mol. Catal.*, **2019**, 476, 110508.

[12] C. Chen, Z. P. Hu, J. T. Ren, S. M. Zhang, Z. Wang, Z. Y. Yuan, *ChemCatChem,* **2019,** 11, 868–877.

[13] D. Zhao, Y. Li, S. Han, Y. Zhang, G. Jiang, Y. Wang, K. Guo, Z. Zhao, C. Xu, R. Li, C. Yu, J. Zhang, B. Ge, E. V. Kondratenko, *iScience*, **2019**, 13, 269–276.

[14] T. Otroshchenko, O. Bulavchenko, H. V. Thanh, J. Rabeah, U. Bentrup, A. Matvienko, U. Rodemerck, B. Paul, R. Kraehnert, D. Linke, E. V. Kondratenko, *Appl. Catal. A*, **2019**, 585, 117189.

[15] Y. Zhang, Y. Zhao, T. Otroshchenko, S. Han, H. Lund, U. Rodemerck, D. Linke, H. Jiao, G. Jiang, E. V. Kondratenko, *J. Catal.*, **2019**, 371, 313–324.

[16] X. Q. Fan, D. D. Liu, Z. Zhao, J. M. Li, J. Liu, *Catal Today,* **2020,** 339, 67–78.

[17] C. Chen, M. L. Sun, Z. P. Hu, Y. P. Liu, S. M. Zhang, Z. Y. Yuan, *Chin. J. Catal.,* **2020,** 41, 276–285.

[18] G. J. Wang, H. Xu, K. Lu, Z. H. Ding, L. C. Bing, *Turk. J. Chem.,* **2020,** 44, 112–125.

[19] M. Nakai, K. Miyake, R. Inoue, K. Ono, H. Al Jabri, Y. Hirota, Y. Uchida, S. Tanaka, M. Miyamoto, Y. Oumi, C.-Y. Kong, N. Nishiyama, *Catal. Sci. Technol.*, **2019**, 9, 6234–6239.

[20] N. M. Phadke, E. Mansoor, M. Bondil, M. Head-Gordon, A. T. Bell, *J. Am. Chem. Soc.,* **2019,** 141, 1614–1627.

[21] Z. Xu, Y. Zhang, X. Wu, H. Zhu, *Chem. Eng. J.* **2025**, 162612.

[22] Y. Dai, J. Gu, S. Tian, Y. Wu, J. Chen, F. Li, Y. Du, L. Peng, W. Ding, Y. Yang, *J. Catal.*, **2020**, 381, 482–492.

[23] L. Liu, H. Li, H. Zhou, S. Chu, L. Liu, Z. Feng, X. Qin, J. Qi, J. Hou, Q. Wu, H. Li, X. Liu, L. Chen, J. Xiao, L. Wang, F.-S. Xiao, *Chem*, **2023**, 9, 637–649.

[24] S. Wei, H. Dai, J. Long, H. Lin, J. Gu, X. Zong, D. Yang, Y. Tang, Y. Yang, Y. Dai, *Chem. Eng. J.*, **2023**, 455, 140726.

[25] B. Hu, A. "Bean" Getsoian, N. M. Schweitzer, U. Das, H. Kim, J. Niklas, O. Poluektov, L. A. Curtiss, P. C. Stair, J. T. Miller, A. S. Hock, *J. Catal.*, **2015**, 322, 24–37.

[26] W. Wang, Y. Wu, T. Liu, Y. Zhao, Y. Qu, R. Yang, Z. Xue, Z. Wang, F. Zhou, J. Long, Z. Yang, X. Han, Y. Lin, M. Chen, L. Zheng, H. Zhou, X. Lin, F. Wu, H. Wang, Y. Yang, Y. Li, Y. Dai, Y. Wu, *ACS Catal.*, **2022**, 12, 2632–2638.

[27] N. Dewangan, J. Ashok, M. Sethia, S. Das, S. Pati, H. Kus, S. Kawi, *ChemCatChem*, **2019**, 11, 4923–4934.

[28] Z.-P. Hu, G. Qin, J. Han, W. Zhang, N. Wang, Y. Zheng, Q. Jiang, T. Ji, Z.-Y. Yuan, J. Xiao, Y. Wei, Z. Liu, *J. Am. Chem. Soc.*, **2022**, 144, 12127–12137.

[29] L. Wu, Z. Ren, Y. He, M. Yang, Y. Yu, Y. Liu, L. Tan, Y. Tang, *ACS Appl.*

Graphical Abstract

Chin. J. Catal., 2025, 74: 108–119 doi: 10.1016/S1872-2067(25)64724-3

Understanding the reaction-induced restructuring of CoO_x species in silicalite-1 to control selectivity in non-oxidative dehydrogenation of propane

Qiyang Zhang *, Vita A. Kondratenko, Xiangnong Ding, Jana Weiss, Stephan Bartling, Elizaveta Fedorova, Dan Zhao, Dmitry E. Doronkin, Dongxu Wang, Christoph Kubis, Evgenii V. Kondratenko *
Leibniz-Institut für Katalyse e.V., Germany; Karlsruhe Institute of Technology, Germany;
Dalian Institute of Chemical Physics, Chinese Academy of Sciences, China; Max Planck Institute of Microstructure Physics, Germany

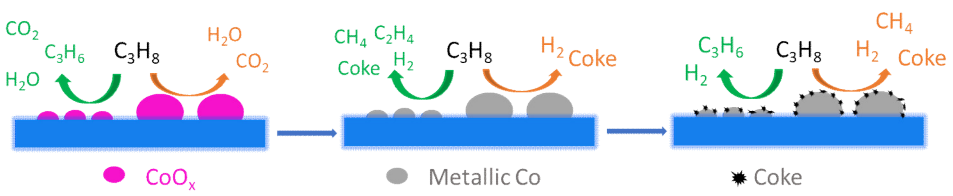

In order to efficiently dehydrogenate propane to propene over CoO_x/Silicalite-1, supported CoO_x species no larger than 2 nm should be reduced in situ to metallic Co^0 and then become decorated with carbon deposits.

Mater. Interfaces, **2021,** 13, 48934–48948.
[30] Chen, S. Zhang, Z. Wang, Z.-Y. Yuan, *J. Catal.*, **2020**, 383, 77–87.
[31] Y. Sun, Y. Wu, H. Shan, C. Li, *Catal. Lett.,* **2015,** 145, 1413–1419.
[32] X. Li, P. Wang, H. Wang, C. Li, *Appl. Surf. Sci.,* **2018,** 441, 688–693
[33] N. Jeon, J. Oh, A. Tayal, B. Jeong, O. Seo, S. Kim, I. Chung, Y. Yun, *J. Catal.,* **2021,** 404, 1007–1016
[34] T. P. Otroshchenko, U. Rodemerck, D. Linke, E. V. Kondratenko, *J. Catal.,* **2017,** 356, 197–205
[35] B. Ravel, M. Newville, *J. Synchrotron Radiat.,* **2005,** 12, 537–541.
[36] J. T. Gleaves, G. S. Yablonskii, P. Phanawadee, Y. Schuurman, *Appl. Catal. A*, **1997**, 160, 55–88.
[37] K. Morgan, N. Maguire, R. Fushimi, J. T. Gleaves, A. Goguet, M. P. Harold, E. V. Kondratenko, U. Menon, Y. Schuurman, G. S. Yablonsky, *Catal. Sci. Technol.*, **2017**, 7, 2416–2439.
[38] J. Perezramirez, E. Kondratenko, *Catal. Today*, **2007**, 121, 160–169.
[39] A. Kuzmin, J. Chaboy, *IUCrJ,* **2014,** 1, 571–589.
[40] S. Lim, D. Ciuparu, Y. Chen, Y. Yang, L. Pfefferle, G. L. Haller, *J. Phys. Chem. B*, **2005**, 109, 2285–2294.
[41] Y. Zhou, L. Liu, G. Li, C. Hu, *ACS Catal.,* **2021,** 11, 7099–7113.
[42] Z. Ren, Y. He, M. Yang, H. Deng, Y. Zhang, H. Yang, Z. Tang, L. Tan, Y. Tang, L. Wu, *Mol. Catal.*, **2022**, 530, 112580.
[43] M. C. Biesinger, B. P. Payne, A. P. Grosvenor, L. W. M. Lau, A. R. Gerson, R. St. C. Smart, *Appl. Surf. Sci.*, **2011**, 257, 2717–2730.
[44] J. T. Gleaves, G. Yablonsky, X. Zheng, R. Fushimi, P. L. Mills, *J. Mol. Catal. A*, **2010**, 315, 108–134.
[45] Z. Huang, D. He, J. Lu, L. Han, K. Li, D. Chen, X. Cao, T. Li, Y. Luo, *Angew. Chem. Int. Ed.*, **2024**, 63, e202408391.
[46] C.-W. Tang, C.-B. Wang, S.-H. Chien, *Thermochim. Acta*, **2008**, 473, 68–73.
[47] M. Bagheri, H. P. Komsa, *J. Raman Spectroscopy*, **2024**, 55, 1113–1123.
[48] A. Sadezky, H. Muckenhuber, H. Grothe, R. Niessner, U. Pöschl, *Carbon*, **2005**, 43, 1731–1742.

Silicalite-1中CoO_x物种在反应诱导下的重构机制以调控丙烷非氧化脱氢选择性

张启扬 [a,*], Vita A. Kondratenko [a], 丁湘浓 [a], Jana Weiss [a], Stephan Bartling [a], Elizaveta Fedorova [a], 赵 丹 [a,b,c], Dmitry E. Doronkin [b], 王东旭 [d], Christoph Kubis [a], Evgenii V. Kondratenko [a,*]

[a]莱布尼茨催化研究所, 罗斯托克, 德国
[b]卡尔斯鲁厄理工学院化学技术与高分子化学研究所, 催化研究与技术研究所, 卡尔斯鲁厄, 德国
[c]中国科学院大连化学物理研究所, 甲醇制烯烃国家工程实验室, 清洁能源国家实验室, 能源材料化学协同创新中心(iChEM), 辽宁大连116023, 中国
[d]马克斯·普朗克微结构物理研究所, 哈勒, 德国

摘要: 丙烷非氧化脱氢(PDH)是大规模定向生产丙烯的重要途径. 尽管钴基催化剂有望替代当前使用的铂基或氧化铬基催化剂, 但由于对目标反应和副反应中活性位点种类的不确定性, 其进一步发展受到限制. 因此, 本文系统研究了基于Silicalite-1分子筛负载的具有不同氧化还原特性的CoO_x物种中氧化态CoO_x和金属态Co^0物种在PDH反应中的作用. 通过亚毫秒级和秒级时间分辨的丙烷脉冲实验(脉冲量分别约13和2200 nmol), 并结合深度的催化剂表征及不同丙烷转化率下的PDH测试, 揭示了反应诱导的CoO_x还原对产物选择性的影响机制. 研究结果表明, 丙烷可快速与CoO_x反应生成丙烯、碳氧化物和水; 生成的Co^0物种在结焦和裂解反应中表现出高活性; 但当此类物种尺寸小于2 nm时, 由于碳物种对活性位点的覆盖显著抑制了这些副反应的发生; 未被覆盖的表面钴位点可选择性催化丙烷脱氢生成丙烯. 性能最优的催化剂展现出高于商用K-CrO_x/Al_2O_3催化剂的活性, 并在工业条件下的10次脱氢/再生循环中保持稳定运行. 在550 °C、平衡丙烷转化率52%和丙烯选择性95%的条件下, 生成丙烯的时空产率达到0.97 $kg \cdot h^{-1} \cdot kg\text{-}cat^{-1}$.

关键词: 丙烷; 脱氢; 丙烯; 钴; 反应机理

收稿日期: 2025-01-28. 接受日期: 2025-03-08. 上网时间: 2025-07-20.

*通讯联系人. 电子信箱: Qiyang.Zhang@catalysis.de (张启扬), Evgenii.kondratenko@catalysis.de (E. V. Kondratenko).